Article

DFT Simulations Investigating the Trapping of Sulfides by 1T-Li$_x$MoS$_2$ and 1T-Li$_x$MoS$_2$/Graphene Hybrid Cathodes in Li-S Batteries

Shumaila Babar [1,2], Elaheh Hojaji [1,2], Qiong Cai [1] and Constantina Lekakou [2,*]

[1] School of Chemistry and Chemical Engineering, University of Surrey, Guildford GU2 7XH, UK; babars@lsbu.ac.uk (S.B.); e.hojaji@surrey.ac.uk (E.H.); q.cai@surrey.ac.uk (Q.C.)

[2] School of Mechanical Engineering Sciences, University of Surrey, Guildford GU2 7XH, UK

* Correspondence: c.lekakou@surrey.ac.uk; Tel.: +44(0)-1483689622

Abstract: The aim of this study is to investigate new materials that can be employed as cathode hosts in Li-S batteries, which would be able to overcome the effect of the shuttling of soluble polysulfides and maximize the battery capacity and energy density. Density functional theory (DFT) simulations are used to determine the adsorption energy of lithium sulfides in two types of cathode hosts: lithiated 1T-MoS$_2$ (1T-Li$_x$MoS$_2$) and hybrid 1T-Li$_x$MoS$_2$/graphene. Initial simulations of lithiated 1T-MoS$_2$ structures led to the selection of an optimized 1T-Li$_{0.75}$MoS$_2$ structure, which was utilized for the formation of an optimized 1T-Li$_{0.75}$MoS$_2$ bilayer and a hybrid 1T-Li$_{0.75}$MoS$_2$/graphene bilayer structure. It was found that all sulfides exhibited super-high adsorption energies in the interlayer inside the 1T-Li$_{0.75}$MoS$_2$ bilayer and very good adsorption energy values in the interlayer inside the hybrid 1T-Li$_{0.75}$MoS$_2$/graphene bilayer. The placement of sulfides outside each type of bilayer, over the 1T-Li$_{0.75}$MoS$_2$ surface, yielded good adsorption energies in the range of -2 to -3.8 eV, which are higher than those over a 1T-MoS$_2$ substrate.

Keywords: DFT simulations; 1T-Li$_{0.75}$MoS$_2$; 1T-Li$_{0.75}$MoS$_2$/graphene hybrid; adsorption energy; activation energy

1. Introduction

Despite the great expectations of high energy density from lithium–sulfur (Li-S) batteries at least in terms of their theoretical capacity, their commercialization is still behind initial predictions due to the fact that these batteries cannot realize their full theoretical capacity and have a limited lifetime [1–3]. The main reason for this is the problem of migration of the soluble sulfur and polysulfides to the anode during discharge and further shuttling between the anode and cathode during charge [4–7]. This occurs for liquid electrolytes in which sulfides Li$_2$S$_x$, x = 4–8, are highly soluble and Li$_2$S$_2$ is partially soluble [8,9]. Hence, different schemes to trap the soluble polysulfides have been devised [10], including electrolyte-lean cells [11–14], sparingly solvating electrolytes that induce a quasi-solid state reaction mechanism [15,16], hollow conductive particles [17–22] or high tortuosity conductive platelets [17] as cathode hosts which delay the transport of polysulfides away from the cathode. Layered graphene platelets have the possibility of high tortuosity [23], but they tend to curl and form large pockets in which sulfur is impregnated and unfortunately from which any soluble sulfides can easily migrate [17,24,25]. Ionic liquid polymer binders that attract polysulfides may also act as trapping means and may be used in meso- and microporous cathode coatings to prevent the migration of polysulfides [26,27]. Alternatively, 1T-MoS$_2$ is another conductive 2D material the nanoplatelets of which might also curl [28,29] but can also form layered, large, conductive platelets [30–33] that can reduce the migration of soluble sulfides via the high tortuosity and high adsorption energy of the

1T-MoS$_2$ which also acts as an excellent electrocatalyst in the electrochemical reactions of Li-S batteries [31].

Functionalizing graphene platelets [34] or other conductive hosts, such as oriented or random carbon nanotubes [35,36], with groups that have high adsorption energy towards sulfides, such as single-atom catalysts [34,36–40] or amines [41], may not have the intended results if the cathode host materials have large mesopores or macropores where the adsorption energy falls as the distance of the sulfide ion increases from the pore wall [42]. As a result, 1T-MoS$_2$-based MXenes still seem a very attractive cathode host due to their long-range lamellar structure with interlayer distances of the order of 1 nm [43,44].

Initial experimental studies [45–47] and molecular modeling in the form of DFT (density functional theory) simulations [48] focused on hexagonal 2H-MoS$_2$ [45,46] or hybrid 2H-MoS$_2$/graphene [49] or reduced graphene oxide (rGO) [50] as cathode host materials for Li-S batteries. It was soon realized that triangular 1T-MoS$_2$ has higher electrical conductivity than 2H-MoS$_2$ which makes it a more preferable cathode host in Li-S batteries on its own [51,52] or anchored on carbon [53,54] in hybrids with graphene [55–57] and also mixed with conductive polymers such as polypyrrole [58]. DFT simulations conducted by our group [31] provided data for the adsorption energies with different lithium sulfides [31,48], preferred conversion pathways from Li$_2$S$_4$ to Li$_2$S and related activation energies for cathode hosts of 1T-MoS$_2$, in pristine form or with one or two sulfur vacancy defects, demonstrating that 1T-MoS$_2$ is very good at trapping liquid polysulfides and is an excellent electrocatalyst for the electrochemical reactions in Li-S batteries [31,59]. This pioneered the development of Li-S batteries with an optimized design of the 1T-MoS$_2$ cathode host in terms of the number of sulfur vacancies in its structure [31] which offered distinct benefits to Li-S technology [31] and sister chemistries [60–62]. It also paved the way for further developments concerning the formation of 1T-Li$_x$MoS$_2$ and its use as a novel cathode host, which yielded a high energy density Li-S battery of 440 Wh/kg of cell for a monolayer pouch cell, with about a 20% higher capacity of cells with the Li$_x$MoS$_2$ cathode host compared to the equivalent cells with the 1T-MoS$_2$ cathode host [63].

Before this most recent development [63], M$_x$MoS$_2$ was proposed as an electrode for monovalent [64,65] or multivalent metal (M)-ion batteries [43,66], on its own [43,64–66] or in the form of carbon or graphene or rGO hybrids [67,68]. The first question has been, of course, the intercalation of metal ions which, in this case, concerns Li$^+$ ions in the MoS$_2$ structure. Different intercalation methods have been studied which produced different interlayer distances, such as electrochemical intercalation [69–71], a solvothermal reaction type of intercalation [72–75] and chemical solution intercalation [76,77], also used in the most successful study for Li-S batteries [63]. Furthermore, for some compositions, a polytype phase transition has been observed upon the intercalation of Li$^+$ ions, forming a stable allotrope of 1T-Li$_x$MoS$_2$ from the 2H phase, where x was varied in the range of 0 to 0.8 [69,77,78]. This observation was confirmed by DFT studies, where the critical content of lithium for the initialization of the 2H to 1T phase transition was reported be x = 0.4 [79,80], with the intercalation energy approaching a plateau for x > 0.6 and reaching a minimum at x = 1 [79]. A benefit of such intercalated structures reported by the DFT simulations is that the expanded interlayer spacing can lower the intercalation energy of further intercalating ions [81,82].

In an attempt to model and simulate the successful Li-S cell [63] to unravel the effect of special features of the Li$_x$MoS$_2$-based cell on the targeted high performance compared to other cathode hosts [17,83–85] and help researchers extend such beneficial features to other cathode materials [86–88], DFT simulations are conducted in this study to provide data for the adsorption energy and reaction activation energy of the high-performance host material with lithium sulfides. The lithium content is specified as x = 0.75, i.e., Li$_{0.75}$MoS$_2$, which ensures the presence of a high proportion of metallic 1T-Li$_{0.75}$MoS$_2$ [89] as demonstrated in the experimental study [63] which is the basis of the present investigation. The investigation starts with a first step of determining the optimum distribution of Li$^+$ ions in a 1T-Li$_{0.75}$MoS$_2$ bilayer structure. It follows with DFT simulations of Li$_2$S$_x$ sulfides,

x = 1,2,4,6,8, encountered in Li-S batteries with typical liquid electrolytes [90–93], in optimized structures with the 1T-Li$_{0.75}$MoS$_2$ bilayer, in the interlayer spacing or over an outer surface of the bilayer. Finally, such DFT simulations are repeated with a hybrid 1T-Li$_{0.75}$MoS$_2$/graphene bilayer to evaluate this lower mass density structure as a potential cathode host for Li-S batteries.

2. Materials and Methods

All structures required to be inputted for the DFT simulations were created, visualized and tested in VESTA and subjected to an initial geometry optimization in Avogadro. The lattice parameters were optimized by allowing the supercell lattice vectors and ionic positions to change in a simulation box with the vacuum space of 35 Å in the Z-direction. Each 1T-MoS$_2$ monolayer was a (4 × 4) 1T-MoS$_2$ supercell of 48 atoms, comprising 16 Mo and 32 S atoms [31]. The graphene layer was a graphene lattice of 50 C atoms.

The Li$_{0.75}$MoS$_2$ bilayer was created from two layers of 1T-MoS$_2$ at an interlayer spacing of 1.14 nm and was geometrically optimized using CASTEP v19.1.1. Starting from a single 1T-MoS$_2$ layer, 12 Li atoms were distributed around the 1T-MoS$_2$ layer to create the 1T-Li$_{0.75}$MoS$_2$ structure. DFT simulations using CASTEP v19.1.1 were employed to identify the optimum structure with the lowest energy, corresponding to the optimum distribution of the Li atoms.

Proceeding to create the Li$_{0.75}$MoS$_2$ bilayer, the interlayer spacing in the 1T-Li$_{0.75}$MoS$_2$ bilayer was 1.14 nm as determined from XRD data in [63], with the MoS$_2$ material exfoliated and lithiated as described in [63,94–96]. In these data (Cu source of wavelength of 0.15418 nm), the single wide peak of MoS$_2$ at 2θ = 14.05° (interlayer spacing of 0.63 nm), upon intercalation with 75 at% Li, was translated into two peaks at an intensity ratio of 4:1. Of these, the major sharp peak at 2θ = 7.75° corresponds to an interlayer spacing of 1.14 nm and represents widened interlayer spacing after Li$^+$ ion intercalation, whereas the low-intensity peak at 2θ = 15.46° corresponds to an interlayer spacing of 0.57 nm which represents non-intercalated MoS$_2$ material which has been compressed by the Li$^+$ intercalation in neighboring interlayers.

Finally, the hybrid bilayer structure of 1T-Li$_{0.75}$MoS$_2$/graphene was created by assembling a layer of 1T-Li$_{0.75}$MoS$_2$ and a layer of graphene. In the absence of further experimental data, the interlayer spacing in the hybrid 1T-Li$_{0.75}$MoS$_2$/graphene bilayer was maintained the same as for the 1T-Li$_{0.75}$MoS$_2$ bilayer, at 1.14 nm, for consistency in the DFT investigation.

CASTEP v19.1.1 was employed to perform all spin-polarized DFT simulations [31,97–99] with a spin polarization of 2. The exchange–correlation potential was calculated using the generalized gradient approximation (GGA) exchange–correlation function as described by Perdew−Burke−Ernzerhof (PBE) [100]. The Brillouin zone was sampled with the Monkhorst–Pack grid using a 2 × 2 × 1 K-point mesh, as optimized for the convergence of the 1T-MoS$_2$ structures in [31] and the structures of the present study. The valence electrons identified on a plane wave basis were used with a cut-off energy of 500 eV. Tight convergence criteria of energy and force tolerance of 10^{-5} eV and 10^{-4} eV/A$°$, respectively, were set to ensure the precision of calculations. The van der Waals (vdW) dispersion correction as described by Grimme's empirical method was further included in all the simulations [101].

Considering a Li-S battery with a typical liquid electrolyte leading to the production of sulfides Li$_2$S$_x$, x = 1, 2, 4, 6, 8, in the cathode [90–93], the adsorption energy of each of these sulfides was determined via DFT simulations for (a) a 1T-Li$_{0.75}$MoS$_2$ bilayer cathode host and (b) a hybrid 1T-Li$_{0.75}$MoS$_2$/graphene bilayer cathode host. Each sulfide was placed either in the interlayer between the two layers or on one side of the bilayer. The adsorption energy, E$_{ads:sulfide-substrate}$, was calculated via the equation from the difference between the energy of the combined structure, E$_{sulfide-substrate}$, and the sum of energies of each individual structure, i.e., E$_{sulfide}$ and E$_{substrate}$:

$$E_{ads:sulfide-substrate} = E_{sulfide-substrate} - (E_{sulfide} + E_{substrate}) \tag{1}$$

To evaluate the catalytic effect of the tested cathode hosts, two alternative disproportionation reaction pathways were investigated for the slow conversion of Li_2S_4 to Li_2S:

(i) A two-step process: $Li_2S_4 \rightarrow Li_2S_2 + S_2$ followed by $Li_2S_2 \rightarrow Li_2S + S$;
(ii) A one-step process: $Li_2S_4 \rightarrow Li_2S + S_3$.

For each of the above reactions, the activation energy (activation barrier) was calculated from the results of the transition state search (TSS) task of a DFT simulation in CASTEP v19.1.1 based on the transition states between the optimized structures of the reactant sulfide in the cathode host and the products in the cathode host. The complete linear synchronous transit and quadratic synchronous transit (LST/QST) methods were used for the TSS task, where the root mean square forces per atom convergence criterion was set to be 10^{-3} eV/Å.

An initial grid parametric study considered DFT and TSS simulations with different sizes of the K-point mesh: $6 \times 6 \times 1$, $4 \times 4 \times 1$ and $2 \times 2 \times 1$. In all simulations, the cut-off energy was 500 eV, the convergence criterion of energy tolerance was 10^{-5} eV and the convergence criterion of force tolerance was 10^{-4} eV/A°. The $2 \times 2 \times 1$ K-point mesh was the only mesh size at which the DFT and TSS simulations of all structures converged, so it was the grid size selected for all structures for consistency to be able to compare the results of adsorption energies and activation energies.

3. Results

3.1. Optimizing the Li Distribution in the 1T-Li$_{0.75}$MoS$_2$ Structure

Starting from the optimized fully relaxed 48-atom 1T-MoS$_2$ monolayer of an energy $E_{1T-MoS2} = -39,651.307$ eV, 12 Li atoms were added gradually. First of all, four sites were considered for the adsorption of a Li atom as shown in Figure 1a: (1) the top site of a S atom in the upper plane, (2) the top site of a Mo atom, (3) the top site of a S atom in the lower plane, and (4) the bridge site above a S–Mo bond, in alignment with first-principles calculations reports [102]. The calculated total energies by the DFT simulations showed that the preferred adsorption site for a Li atom was over the top of a Mo atom (site 2 in Figure 1a) with a little deviation from the structure with the Li over a Mo–S bond.
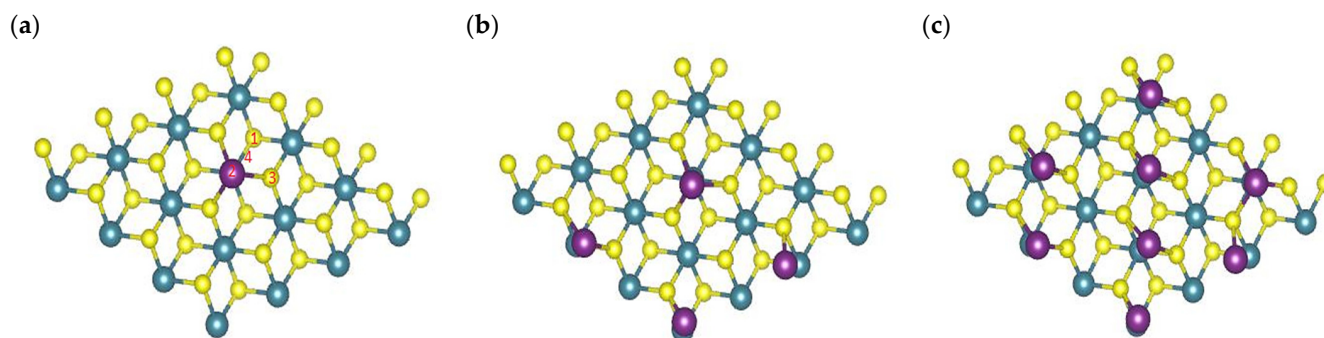

Figure 1. Optimized structures of Li$_x$MoS$_2$ with different number of Li atoms adsorbed over one side of 48-atom 1T-MoS$_2$ monolayer: (**a**) one Li atom, (**b**) four Li atoms, (**c**) eight Li atoms.

The further addition of three Li atoms favored the bridge site above a S–Mo bond of next nearest neighboring Mo atoms, with a minimum Li-Li distance of 5.7 Å and Li-S distance of 2.7 Å as seen in Figure 1b. The addition of the fifth, sixth, seventh and eighth Li atoms followed similar trends, with the Li atoms close to sites over the nearest neighboring Mo atoms, with Li-S distance of 2.7 Å. Figure 1c depicts the structure with eight Li atoms on the same side with an obvious distortion of the structure of the 1T-MoS$_2$ monolayer. It was noticed that increasing the number of the adsorbed Li atoms on one side of the 1T-MoS$_2$ monolayer resulted in a lower structure energy. The rest of the four Li atoms were added on the other side of the 1T-MoS$_2$ monolayer following a similar optimization procedure, resulting in the structure displayed in Figure 2.
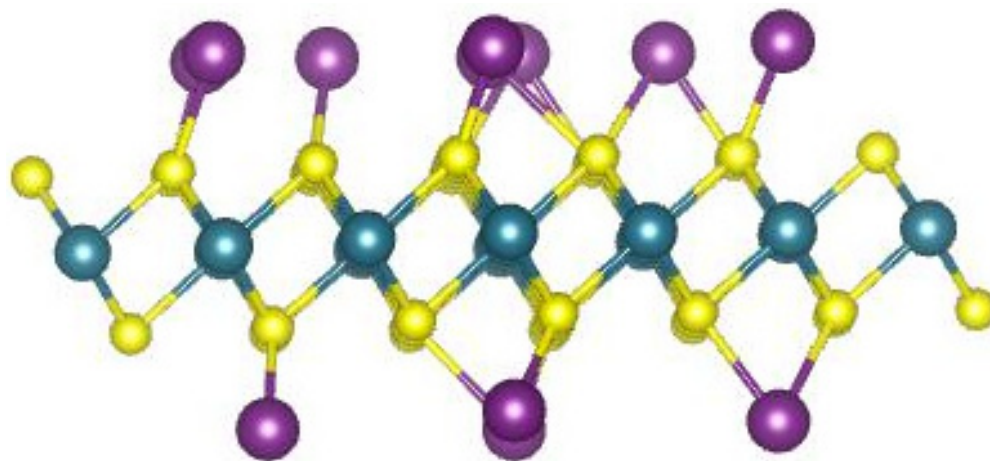
Figure 2. Optimized structure of 1T-$Li_{0.75}MoS_2$ monolayer.

3.2. DFT Similations of the 1T-$Li_{0.75}MoS_2$ Bilayer as Cathode Host in Li-S Batteries

Combining two monolayer structures as in Figure 2 with an interlayer spacing of 1.14 nm, as determined from XRD data [63], the optimized 1T-$Li_{0.75}MoS_2$ bilayer structure is presented in Figure 3a (same as Figure 4a), with a total calculated energy of $E_{1T-Li0.75MoS2\ bilayer} = -84,196.343$ eV. The sulfides Li_2S_x, x = 1, 2, 4, 6, 8, were placed either inside or outside the 1T-$Li_{0.75}MoS_2$ bilayer structure, and the optimized structures are presented in Figures 3b–f and 4b–f, respectively. Table 1 depicts the resulted adsorption energies for each sulfide inside or outside the 1T-$Li_{0.75}MoS_2$ bilayer structure and compares them with the corresponding adsorption energy values with respect to the 1T-MoS_2 cathode host. It is clear that the 1T-$Li_{0.75}MoS_2$ bilayer structure traps the soluble sulfides much better than the 1T-MoS_2 host, especially in the interlayer, inside the 1T-$Li_{0.75}MoS_2$ bilayer structure.
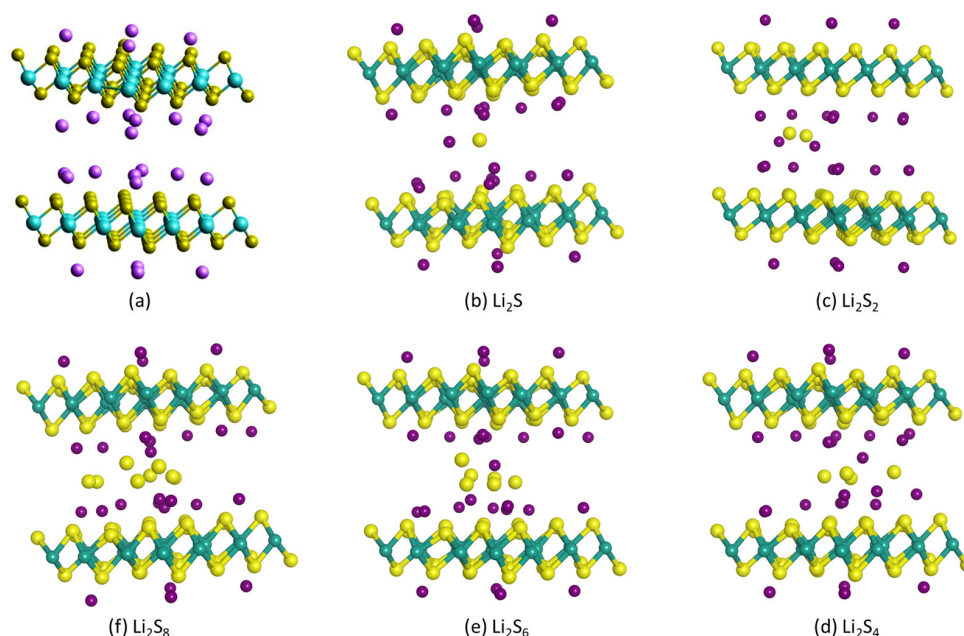

(a)

(b) Li_2S

(c) Li_2S_2

(f) Li_2S_8

(e) Li_2S_6

(d) Li_2S_4

Figure 3. Optimized structures of (**a**) 1T-$Li_{0.75}MoS_2$ bilayer and (**b**–**f**) 1T-$Li_{0.75}MoS_2$ bilayer with a Li_2S_x sulfide between the two 1T-$Li_{0.75}MoS_2$ layers.
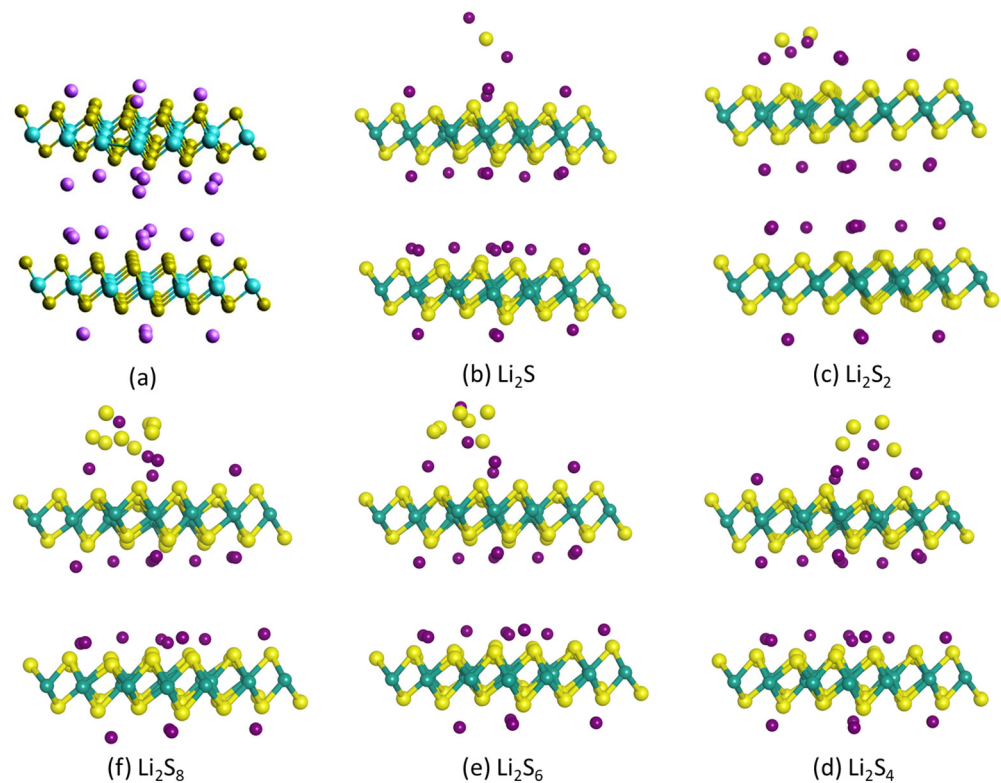
Figure 4. Optimized structures of (**a**) 1T-$Li_{0.75}MoS_2$ bilayer and (**b**–**f**) 1T-$Li_{0.75}MoS_2$ bilayer with a Li_2S_x sulfide outside the 1T-$Li_{0.75}MoS_2$ bilayer.

Table 1. Adsorption energies of each lithium sulfide inside or outside the 1T-$Li_{0.75}MoS_2$ bilayer compared to the corresponding adsorption energies of each lithium sulfide over a 1T-MoS_2 monolayer [31].

Sulfide	Inside 1T-$Li_{0.75}MoS_2$ (In the Interlayer) E_{ads} (eV)	Outside 1T-MoS_2 E_{ads} (eV)	Outside 1T-MoS_2 E_{ads} (eV)
Li_2S	−3.05	−2.07	−3.30
Li_2S_2	−6.50	−2.11	−2.42
Li_2S_4	−8.25	−1.99	−2.23
Li_2S_6	−6.85	−2.54	−0.96
Li_2S_8	−12.54	−3.77	−0.77

The obtained reaction activation energies, E_{ra}, for the reactions of the two alternative pathways for the conversion from Li_2S_4 to Li_2S indicated that the preferred pathway with the lowest E_{ra} value was, in all cases, the one-step process:

$$Li_2S_4 \rightarrow Li_2S + S_3$$
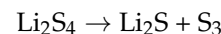
with the E_{ra} values presented in Table 2, where it can be seen that the pure reaction activation energy either inside or outside the 1T-$Li_{0.75}MoS_2$ bilayer is higher than that on the 1T-MoS_2 cathode host. However, one may consider this process as a combination of a first adsorption step in which Li_2S_4 is adsorbed at the catalytic site of the cathode host and a second reaction step [103]. Therefore, the whole activation energy, E_a, is considered as the sum of E_{ra} and E_{ads}. The E_a values presented in Table 2 indicate that, overall, the adsorption and reaction process has the lowest energy in the interlayer of 1T-$Li_{0.75}MoS_2$.

Table 2. Activation energies of the one-step process: $Li_2S_4 \rightarrow Li_2S + S_3$ inside or outside the 1T-$Li_{0.75}MoS_2$ bilayer compared to the corresponding energies over a 1T-MoS_2 monolayer [31].

Cathode Host	E_{ra} (eV)	$E_{ads,Li2S4}$ (eV)	E_a (eV)
Inside 1T-$Li_{0.75}MoS_2$	6.50	−8.25	−1.75
Outside 1T-$Li_{0.75}MoS_2$	2.77	−1.99	0.78
Outside 1T-MoS_2	1.73	−2.23	−0.50

3.3. DFT Similations of the Hybrid 1T-$Li_{0.75}MoS_2$/Graphene Bilayer as Cathode Host in Li-S Batteries

Figure 5a depicts the hybrid 1T-$Li_{0.75}MoS_2$/graphene bilayer which has been formed by keeping the same interlayer distance of 1.14 nm as in the 1T-$Li_{0.75}MoS_2$ bilayer in Figures 3a and 4a. The sulfides Li_2S_x, x = 1, 2, 4, 6, 8, were placed either inside the hybrid structure in the interlayer between the 1T-$Li_{0.75}MoS_2$ and graphene layers, as in Figure 5b–f, or outside over the 1T-$Li_{0.75}MoS_2$ layer, as in Figure 6b–f, or outside over the graphene layer, as in Figure 7b–f. Table 3 presents the adsorption energies of each of these lithium sulfides for each configuration and the adsorption energies of each corresponding sulfide over a 1T-MoS_2 layer and over a graphene layer. It seems that the adsorption energies of soluble sulfides inside the hybrid bilayer are lower than those for the corresponding sulfides inside the 1T-$Li_{0.75}MoS_2$ bilayer but higher than those outside the 1T-MoS_2 layer or the graphene layer. The adsorption energies of the soluble sulfides outside the 1T-$Li_{0.75}MoS_2$ layer are similar to those of the corresponding sulfides outside the 1T-$Li_{0.75}MoS_2$ bilayer in Table 1 but higher than those outside the 1T-MoS_2 layer. The adsorption energies of the soluble sulfides outside the graphene layer of the hybrid 1T-$Li_{0.75}MoS_2$/graphene bilayer in Table 3 are similar to those of the corresponding sulfides outside the pure graphene layer in Table 3.

(a)

(b) Li_2S

(c) Li_2S_2

(f) Li_2S_8

(e) Li_2S_6

(d) Li_2S_4
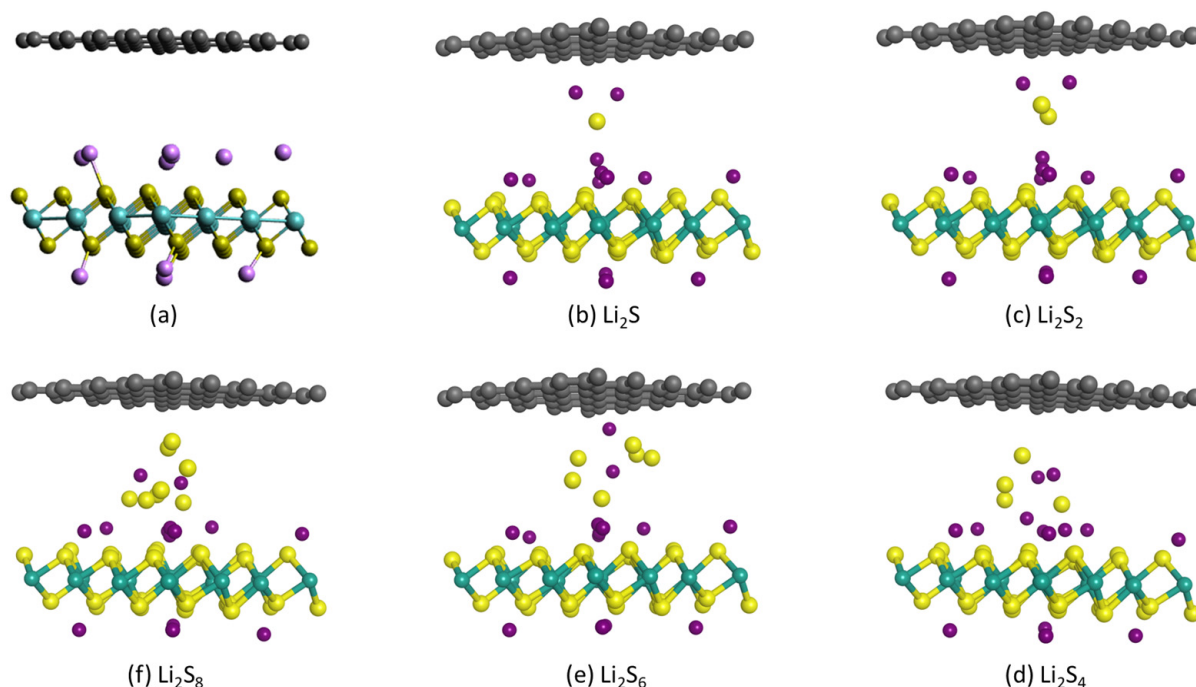
Figure 5. Optimized structures of (**a**) hybrid 1T-$Li_{0.75}MoS_2$/graphene bilayer and (**b–f**) 1T-$Li_{0.75}MoS_2$/graphene bilayer with a Li_2S_x sulfide between the 1T-$Li_{0.75}MoS_2$ and the graphene layers.

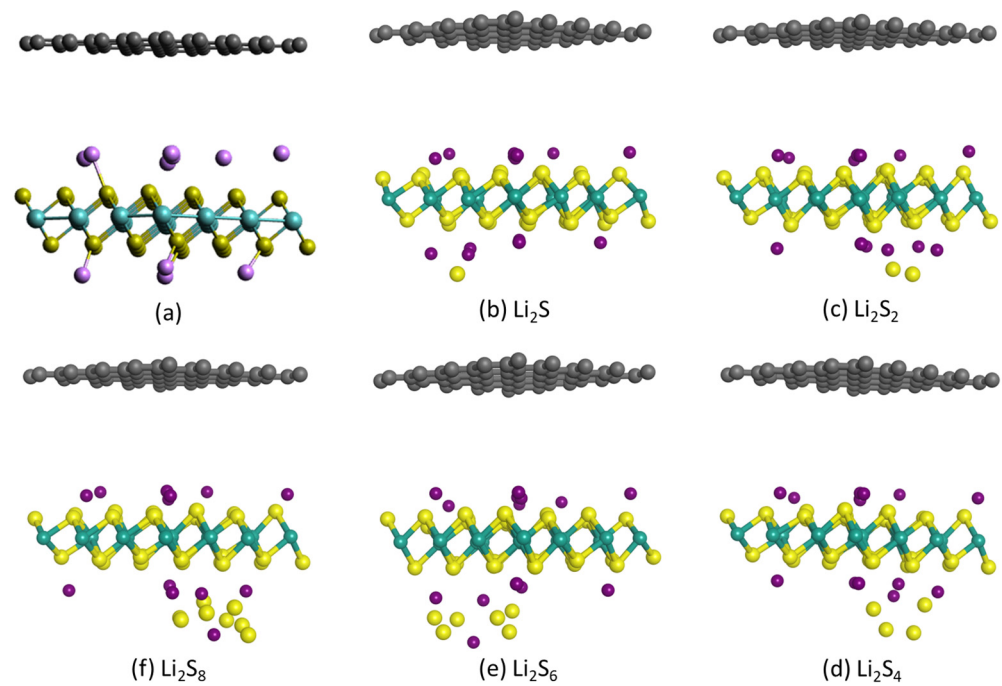**Figure 6.** Optimized structures of (**a**) hybrid 1T-Li$_{0.75}$MoS$_2$/graphene bilayer and (**b**–**f**) 1T-Li$_{0.75}$MoS$_2$/graphene bilayer with a Li$_2$S$_x$ sulfide outside the 1T-Li$_{0.75}$MoS$_2$ layer.
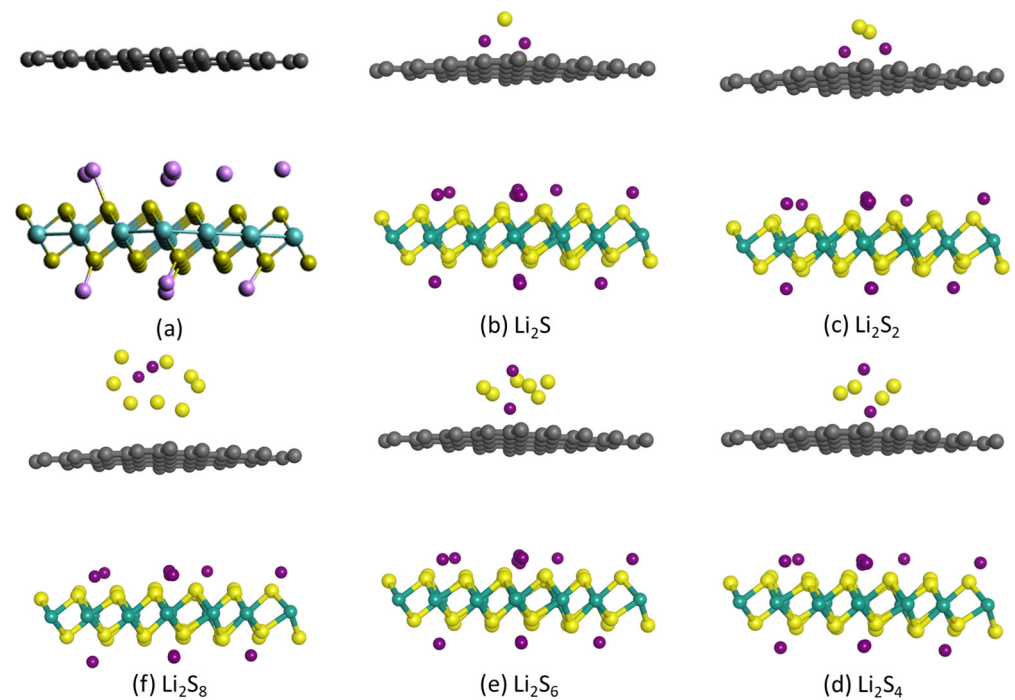
Figure 7. Optimized structures of (**a**) hybrid 1T-Li$_{0.75}$MoS$_2$/graphene bilayer and (**b**–**f**) 1T-Li$_{0.75}$MoS$_2$/graphene bilayer with a Li$_2$S$_x$ sulfide outside the graphene layer.

Table 3. Adsorption energies of each lithium sulfide inside or outside the hybrid 1T-$Li_{0.75}MoS_2$/graphene bilayer compared to the corresponding adsorption energies of each lithium sulfide over a 1T-MoS_2 monolayer [31] and a graphene monolayer [34].

Sulfide	Inside Bilayer (In Interlayer) E_{ads} (eV)	Outside 1T-$Li_{0.75}MoS_2$ E_{ads} (eV)	Outside Graphene E_{ads} (eV)	Over 1T-MoS_2 E_{ads} (eV)	Over Graphene E_{ads} (eV)
Li_2S	−1.76	−2.54	−1.05	−3.30	−1.11
Li_2S_2	−1.55	−2.45	−1.28	−2.42	−1.01
Li_2S_4	−5.24	−2.34	−0.66	−2.23	−0.69
Li_2S_6	−2.32	−2.26	−0.88	−0.96	−0.87
Li_2S_8	−5.73	−2.03	−0.96	−0.77	−0.71

4. Discussion and Conclusions

The Li intercalation step in Section 3.1 offers valuable novel contributions in the literature, not only for Li-S batteries but also for Li-ion batteries. The finally optimized structure of the 1T-$Li_{0.75}MoS_2$ monolayer in Figure 2 is different from symmetrically distributed Li atoms on either side of 1T-MoS_2 in the literature ([79], for example), with eight Li atoms on one side (inner side in the bilayer) and four Li atoms on the other side (outer side of the bilayer) in this study. The selection of this structure in this study was based on the process of introducing the Li atoms sequentially and structure optimization after each step of introduction, which resulted in lower energy each time as up to eight Li atoms were introduced on one side. Furthermore, the interlayer distance of 1.14 nm in the 1T-$Li_{0.75}MoS_2$ bilayer in this study was specified on the basis of experimental XRD data [63].

The DFT investigations of the 1T-$Li_{0.75}MoS_2$ bilayer in relation to lithium sulfides and their reactions have provided novel data and useful insights for 1T-$Li_{0.75}MoS_2$ as the cathode host in Li-S batteries. The focus on the challenge of trapping the sulfides is on the highly soluble sulfides in liquid electrolytes, which include Li_2S_4, Li_2S_6 and Li_2S_8 [8,9] and how the cathode hosts investigated in this study compare with other cathode hosts for Li-S batteries. For sulfides over the outer surface of the 1T-$Li_{0.75}MoS_2$ bilayer, the adsorption energies presented in Table 1 for the soluble sulfides Li_2S_8 and Li_2S_6 are higher than their adsorption energies caused by 1T-MoS_2. Additionally, the adsorption energies of all soluble lithium sulfides over the outer surface of the 1T-$Li_{0.75}MoS_2$ bilayer in Table 1 are higher than those caused by single-atom catalysts Fe-N_4-C and Co-N_4-C reported in [34] but not by V-N_4-C and W-N_4-C [34]. However, the DFT simulation results reported in Tables 1 and 3 demonstrate the super-high adsorption energies of all soluble sulfides in the interlayer inside the 1T-$Li_{0.75}MoS_2$ bilayer compared to all the other structures examined in this study, to 1T-MoS_2 [31] and also to many single-atom catalysts such as Fe-N_4-C, Co-N_4-C, V-N_4-C and W-N_4-C [34]. This has been confirmed in an experimental study of Li_2S_4 adsorption from electrolyte solution for different cathode hosts, including 1T-$Li_{0.75}MoS_2$ [63], and the high Li-S battery performance with this cathode host [63].

One of the reasons for the higher adsorption energy of the lithium sulfides in the interlayer inside the 1T-$Li_{0.75}MoS_2$ bilayer is the additive effect of the superimposed adsorption energies caused by the two 1T-$Li_{0.75}MoS_2$ monolayers on either side. However, it is noticed that the adsorption energy of the lithium sulfides in the interlayer is 3–4 times the adsorption energy of these sulfides on the outer layer, i.e., well more than double. We believe that the reason for such a high adsorption energy is that the S atoms of the sulfides are bonded not only with the Li atoms of Li_2S_x but are also shared by the intercalated Li atoms in the 1T-$Li_{0.75}MoS_2$ bilayer that are at a higher density in the interlayer than on the outer surface (only four Li atoms on each outer surface). This is also the reason for the higher adsorption energies in the 1T-$Li_{0.75}MoS_2$ bilayer than over 1T-MoS_2.

The DFT-aided evaluation of the hybrid 1T-$Li_{0.75}MoS_2$/graphene bilayer is another novel feature of this study, where the advantage of graphene is its low density compared to MoS_2, the density of which is more than double the density of graphene. Tables 1 and 3 reveal that the hybrid 1T-$Li_{0.75}MoS_2$/graphene bilayer has very good but not so high ad-

sorption energies of the soluble sulfides inside the bilayer which may still lead to the trapping of soluble sulfides. The high adsorption of lithium sulfides caused by 1T-Li$_{0.75}$MoS$_2$ compared to graphene can be attributed to two reasons: (a) the sharing of the Li atoms of the sulfides by the S atoms of MoS$_2$, which are the lithiophilic (as well as hydrophilic [55]) sites of MoS$_2$; and (b) the sharing of the S atoms of the sulfides by the intercalated Li in 1T-Li$_{0.75}$MoS$_2$.

The other important issue is the catalytic role of the cathode host. The high adsorption energy of a reactant caused by a catalyst may favor the attraction of the reactant to the catalytic site and ultimately lower the reaction activation energy [104]. However, there is an optimum adsorption energy value for species under reduction [105,106], such as sulfur, sulfides or oxygen, above which the species is too strongly adsorbed on the substrate site to participate in further reduction reactions, in which case the reaction activation energy is not reduced. This explains how the super-high adsorption energy of Li$_2$S$_4$ inside the 1T-Li$_{0.75}$MoS$_2$ bilayer (E$_{ads}$ = −8.25 eV) in Table 1 yields a rather high reaction activation energy of E$_{ra}$ = 6.5 eV in Table 3 for the conversion of Li$_2$S$_4$ to Li$_2$S. Li et al. [63] derived activation energies for the lithium sulfide conversion chain in Li-S batteries from the variation in the charge transfer resistance with temperature at different battery cell voltages. From their experimental data [63], it can be concluded that the maximum activation energy for the low-voltage plateau reaction(s) (conversion of Li$_2$S$_4$ to Li$_2$S) is the lowest at 0.1 eV for the 1T-Li$_{0.75}$MoS$_2$ cathode host compared to 0.15 eV for the 1T-MoS$_2$ cathode host. Hence, it was thought, in the present study, that the sum of adsorption and reaction activation energies would be more representative of the total activation energy [103]. This resulted in the E$_{ads}$ + E$_{ra}$ values reported in Table 2, which confirms the trend that, overall, the 1T-Li$_{0.75}$MoS$_2$ cathode host has a lower total activation energy than the 1T-MoS$_2$ host. The improved electrocatalyst properties of 1T-Li$_{0.75}$MoS$_2$ are expected to reduce the overpotential of the Li-S battery cell, which would enable the cell to operate at higher C rates.

The contribution of the DFT simulations in this study is providing data of adsorption energies, the optimum reaction pathway and the reaction activation energy regarding the 1T-Li$_{0.75}$MoS$_2$ and the hybrid 1T-Li$_{0.75}$MoS$_2$/graphene structure as cathode hosts in Li-S batteries. In terms of trapping the soluble polysulfides, the DFT simulations concluded that the 1T-Li$_{0.75}$MoS$_2$ bilayer has a higher adsorption energy than the hybrid 1T-Li$_{0.75}$MoS$_2$/graphene structure, which, however, has better adsorption energies than mere graphene. However, although these values of adsorption energies are encouraging, they do not tell the full story demonstrating the high performance and cyclability of the corresponding Li-S batteries.

The microstructure of the porous cathode host is equally important in Li-S batteries. While micropores and hollow particles hold the sulfides and sulfur and prevent their migration to the anode, open meso- and macropores let the sulfides escape to the anode [17]. Hence, large-size pores need the high adsorption energy and would most benefit from 1T-Li$_{0.75}$MoS$_2$. The adsorption energy fades with the distance away from the pore walls, where the adsorption energies of 1T-Li$_{0.75}$MoS$_2$ fall to the level of a graphene wall for 1T-Li$_{0.75}$MoS$_2$ mesopore widths as follows: a 9 nm pore has E$_{ads}$ = −0.7 eV for Li$_2$S$_8$, a 4 nm pore has E$_{ads}$ = −0.85 eV for Li$_2$S$_6$ and E$_{ads}$ = −0.9 eV for Li$_2$S$_2$ and a 6 nm pore has E$_{ads}$ = −0.6 eV for Li$_2$S$_4$; larger pores will have even lower adsorption energies towards the soluble sulfides. The electrocatalytic effect can of course be considered only if the sulfides are in close distance with the pore walls of the 1T-Li$_{0.75}$MoS$_2$ materials.

Therefore, further experimental studies or continuum model-based simulations, taking into account the pore size distribution and tortuosity of the structure [17], are needed to assess the 1T-Li$_{0.75}$MoS$_2$ cathode host and the hybrid 1T-Li$_{0.75}$MoS$_2$/graphene cathode host in Li-S batteries, with regards to the trapping of polysulfides and the battery performance. The benefit of the present study is that it will contribute the data of the adsorption energies and reaction activation energies to be used as input data in the continuum simulations, taking into account multiple factors, including the microstructure of cathodes, adsorption energies and electrocatalytic effects of pore walls. The adsorption energies of the hybrid

1T-Li$_{0.75}$MoS$_2$/graphene structure will also be useful in continuum simulations and in providing insights beyond graphene monolayers, such as 1T-Li$_{0.75}$MoS$_2$-coated carbon fabric [107,108].

Supplementary Materials: The following supporting information can be downloaded at: https://www.mdpi.com/article/10.3390/batteries10040124/s1, LixMoS2_graphene_SI1.xyz: xyz.datafile of optimized structure Li0.75MoS2/graphene.

Author Contributions: Conceptualization, Q.C. and C.L.; methodology, S.B., E.H., Q.C. and C.L.; software, S.B., E.H. and C.L.; validation, S.B., E.H. and C.L.; formal analysis, S.B., E.H. and C.L.; investigation, S.B., E.H. and C.L.; resources, Q.C. and C.L.; data curation, Q.C. and C.L.; writing—original draft preparation, S.B., E.H. and C.L.; writing—review and editing, C.L. and Q.C.; visualization, S.B., E.H. and C.L.; supervision, Q.C. and C.L.; project administration, C.L.; funding acquisition, C.L. All authors have read and agreed to the published version of the manuscript.

Data Availability Statement: All data are made available in this study. Additionally, the data of the optimized structure of the hybrid 1T-Li$_{0.75}$MoS$_2$-graphene are given as xyz file dataset in the Supplementary Materials File. Any further data will become available upon reasonable request.

Conflicts of Interest: The authors declare no conflicts of interest.

References

1. Zhu, K.; Wang, C.; Chi, Z.; Ke, F.; Yang, Y.; Wang, A.; Wang, W.; Miao, L. How far away are lithium-sulfur batteries from commercialization? *Front. Energy Res.* **2019**, *7*, 00123. [CrossRef]
2. Tokur, M. A Promising Approach towards the commercialization of lithium sulfur batteries: Prelithiated graphene. *ChemistrySelect* **2023**, *8*, e202302576. [CrossRef]
3. Kumar, R.; Liu, J.; Hwang, J.-Y.; Sun, Y.-K. Recent research trends in Li–S batteries. *J. Mater. Chem. A* **2018**, *6*, 11582–11605. [CrossRef]
4. Mistry, A.N.; Mukherjee, P.P. "Shuttle" in polysulfide shuttle: Friend or foe? *J. Phys. Chem. C* **2018**, *122*, 23845–23851. [CrossRef]
5. Huang, Y.; Lin, L.; Zhang, C.; Liu, L.; Li, Y.; Qiao, Z.; Lin, J.; Wei, Q.; Wang, L.; Xie, Q.; et al. Recent advances and strategies toward polysulfides shuttle inhibition for high-performance Li–S batteries. *Adv. Sci.* **2022**, *9*, 2106004. [CrossRef]
6. Song, Y.-X.; Shi, Y.; Wan, J.; Lang, S.-Y.; Hu, X.-C.; Yan, H.-J.; Liu, B.; Guo, Y.-G.; Wen, R.; Wan, L.-J. Direct tracking of the polysulfide shuttling and interfacial evolution in all-solid-state lithium–sulfur batteries: A degradation mechanism study. *Energy Environ. Sci.* **2019**, *12*, 2496–2506. [CrossRef]
7. Moy, D.; Manivannan, A.; Narayanan, S.R. Direct measurement of polysulfide shuttle current: A window into understanding the performance of lithium-sulfur cells. *J. Electrochem. Soc.* **2015**, *162*, A1. [CrossRef]
8. Dent, M.; Jakubczyk, E.; Zhang, T.; Lekakou, C. Kinetics of sulphur dissolution in lithium–sulphur batteries. *J. Phys. Energy* **2022**, *4*, 024001. [CrossRef]
9. Adeoye, H.A.; Dent, M.; Watts, J.F.; Tennison, S.; Lekakou, C. Solubility and dissolution kinetics of sulfur and sulfides in electrolyte solvents for lithium–sulfur and sodium–sulfur batteries. *J. Chem. Phys.* **2023**, *158*, 064702. [CrossRef]
10. Zhu, Y.; Chen, Z.; Chen, H.; Fu, X.; Awuye, D.E.; Yin, X.; Zhao, Y. Breaking the barrier: Strategies for mitigating shuttle effect in lithium–sulfur batteries using advanced separators. *Polymers* **2023**, *15*, 3955. [CrossRef]
11. Dent, M.; Grabe, S.; Lekakou, C. The challenge of electrolyte impregnation in the fabrication and operation of Li-ion and Li-S batteries. *Batter. Supercaps* **2023**, *7*, e202300327. [CrossRef]
12. Ye, H.; Li, Y. Towards practical lean-electrolyte Li–S batteries: Highly solvating electrolytes or sparingly solvating electrolytes? *Nano Res. Energy* **2022**, *1*, 9120012. [CrossRef]
13. Zhao, M.; Li, B.-Q.; Peng, H.-J.; Yuan, H.; Wei, J.-Y.; Huang, J.-Q. Lithium–sulfur batteries under lean electrolyte conditions: Challenges and opportunities. *Angew. Chem.* **2020**, *59*, 12636–12652. [CrossRef] [PubMed]
14. Jeoun, Y.; Kim, M.-S.; Lee, S.-H.; Um, J.H.; Sung, Y.-E.; Yu, S.-H. Lean-electrolyte lithium-sulfur batteries: Recent advances in the design of cell components. *Chem. Eng. J.* **2022**, *450*, 138209. [CrossRef]
15. Castillo, J.; Soria-Fernández, A.; Rodriguez-Peña, S.; Rikarte, J.; Robles-Fernández, A.; Aldalur, I.; Cid, R.; González-Marcos, J.A.; Carrasco, J.; Armand, M.; et al. Graphene-based sulfur cathodes and dual salt-based sparingly solvating electrolytes: A perfect marriage for high performing, safe, and long cycle life lithium-sulfur prototype batteries. *Adv. Energy Mater.* **2024**, *14*, 2302378. [CrossRef]

16. Liu, J.; Li, S.; Nomura, N.; Ueno, K.; Dokko, K.; Watanabe, M. Enhancing Li–S battery performance with limiting Li[N(SO$_2$F)$_2$] content in a sulfolane-based sparingly solvating electrolyte. *ACS Appl. Mater. Interfaces* **2024**, *16*, 8570–8579. [CrossRef] [PubMed]
17. Grabe, S.; Dent, M.; Zhang, T.; Tennison, S.; Lekakou, C. A physicochemical model-based digital twin of Li–S batteries to elucidate the effects of cathode microstructure and evaluate different microstructures. *J. Power Sources* **2023**, *580*, 233470. [CrossRef]
18. Jayaprakash, N.; Shen, J.; Moganty, S.S.; Corona, A.; Archer, L.A. Porous hollow carbon-sulfur composites for high-power lithium–sulfur batteries. *Angew. Chem. Int. Ed.* **2011**, *50*, 5904–5908. [CrossRef]
19. He, G.; Evers, S.; Liang, X.; Cuisinier, M.; Garsuch, A.; Nazar, L.F. Tailoring porosity in carbon nanospheres for lithium-sulfur battery cathodes. *ACS Nano* **2013**, *7*, 10920–10930. [CrossRef]
20. Li, M.; Zhang, Y.; Wang, X.; Ahn, W.; Jiang, G.; Feng, K.; Lui, G.; Chen, Z. Gas pickering emulsion templated hollow carbon for high rate performance lithium sulfur batteries. *Adv. Funct. Mater.* **2016**, *26*, 8408–8417. [CrossRef]
21. Chen, M.; Su, Z.; Jiang, K.; Pan, Y.; Zhang, Y.; Long, L. Promoting sulfur immobilization by a hierarchical morphology of hollow carbon nanosphere clusters for high-stability Li–S battery. *J. Mater. Chem. A* **2019**, *7*, 6250–6258. [CrossRef]
22. Ding, X.; Jin, J.; Huang, X.; Zhou, S.; Xiao, A.; Chen, Y.; Zuo, C. An in situ template for the synthesis of tunable hollow carbon particles for high-performance lithium−sulfur batteries. *ACS Omega* **2019**, *4*, 16088–16094. [CrossRef]
23. Baboo, J.P.; Babar, S.; Kale, D.; Lekakou, C.; Laudone, G.M. Designing a graphene coating-based supercapacitor with lithium ion electrolyte: An experimental and computational study via multiscale modeling. *Nanomaterials* **2021**, *11*, 2899. [CrossRef]
24. Reece, R.; Lekakou, C.; Smith, P.A.; Grilli, R.; Trapalis, C. Sulphur-linked graphitic and graphene oxide platelet-based electrodes for electrochemical double layer capacitors. *J. Alloys Compd.* **2019**, *792*, 582–593. [CrossRef]
25. Vermisoglou, E.C.; Giannakopoulou, T.; Romanos, G.; Boukos, N.; Psycharis, V.; Lei, C.; Lekakou, C.; Petridis, D.; Trapalis, C. Graphene-based materials via benzidine-assisted exfoliation and reduction of graphite oxide and their electrochemical properties. *Appl. Surf. Sci.* **2017**, *392*, 244–255. [CrossRef]
26. Santiago, A.; Robles-Fernández, A.; Soria-Fernández, A.; Lopez-Morales, J.L.; Castillo, J.; Fraile-Insagurbe, D.; Casado, N.; Armand, M.; Garcia-Suarez, E.J.; Carriazo, D. Polymeric ionic liquid as binder: A promising strategy for enhancing Li–S battery performance. *J. Energy Storage* **2024**, *80*, 110285. [CrossRef]
27. Vizintin, A.; Guterman, R.; Schmidt, J.; Antonietti, M.; Dominko, R. Linear and cross-linked ionic liquid polymers as binders in lithium–sulfur batteries. *Chem. Mater.* **2018**, *30*, 5444–5450. [CrossRef]
28. Tian, L.; Wu, R.; Liu, H.Y. Synthesis of Au-nanoparticle-loaded 1T@2H-MoS$_2$ nanosheets with high photocatalytic performance. *Energy Mater.* **2019**, *54*, 9656–9665. [CrossRef]
29. Li, L.; Chen, J.; Wu, K.; Cao, C.; Shi, S.; Cui, J. The stability of metallic MoS$_2$ nanosheets and their property change by annealing. *Nanomaterials* **2019**, *9*, 1366. [CrossRef]
30. Wang, L.; Zhang, X.; Xu, Y.; Li, C.; Liu, W.; Yi, S.; Wang, K.; Sun, X.; Wu, Z.-S.; Ma, Y. Tetrabutylammonium-intercalated 1T-MoS$_2$ nanosheets with expanded interlayer spacing vertically coupled on 2D delaminated MXene for high-performance lithium-ion capacitors. *Adv. Funct. Mat.* **2021**, *31*, 2104286. [CrossRef]
31. Hojaji, E.; Andritsos, E.I.; Li, Z.; Chhowalla, M.; Lekakou, C.; Cai, Q. DFT Simulation-based design of 1T-MoS$_2$ cathode hosts for Li-S batteries and experimental evaluation. *Int. J. Mol. Sci.* **2022**, *23*, 15608. [CrossRef]
32. Guo, Y.; Dun, C.; Xu, J.; Li, P.; Huang, W.; Mu, J.; Hou, C.; Hewitt, C.A.; Zhang, Q.; Li, Y.; et al. Wearable thermoelectric devices based on Au-decorated two-dimensional MoS$_2$. *ACS Appl. Mater. Interfaces* **2018**, *10*, 33316–33321. [CrossRef]
33. Wang, L.; Li, J.; Zhou, H.; Huang, Z.; Zhai, B.; Liu, L.; Hu, L. Three-dimensionally layers nanosheets of MoS$_2$ with enhanced electrochemical performance using as free-standing anodes of lithium ion batteries. *J. Mater. Sci. Mater. Electron.* **2018**, *29*, 3110–3119. [CrossRef]
34. Andritsos, E.I.; Lekakou, C.; Cai, Q. Single-atom catalysts as promising cathode materials for lithium–sulfur batteries. *J. Phys. Chem. C* **2021**, *125*, 18108–18118. [CrossRef]
35. Murugesh, A.K.; Uthayanan, A.; Lekakou, C. Electrophoresis and orientation of multiple wall carbon nanotubes in polymer solution. *Appl. Phys. A* **2010**, *100*, 135–144. [CrossRef]
36. Zhang, Y.; Liu, J.; Wang, J.; Zhao, Y.; Luo, D.; Yu, A.; Wang, X.; Chen, Z. Engineering oversaturated Fe-N5 multifunctional catalytic sites for durable lithium-sulfur batteries. *Angew. Chem. Int. Ed.* **2021**, *60*, 26622–26629. [CrossRef]
37. Zhao, H.; Tian, B.; Su, C.; Li, Y. Single-atom iron and doped sulfur improve the catalysis of polysulfide conversion for obtaining high-performance lithium–sulfur batteries. *ACS Appl. Mater. Interfaces* **2021**, *13*, 7171–7177. [CrossRef]
38. Wang, J.; Qiu, W.; Li, G.; Liu, J.; Luo, D.; Zhang, Y.; Zhao, Y.; Zhou, G.; Shui, L.; Wang, X.; et al. Coordinatively deficient single-atom Fe-N-C electrocatalyst with optimized electronic structure for high-performance lithium-sulfur batteries. *Energy Storage Mater.* **2022**, *46*, 269–277. [CrossRef]
39. Sun, X.; Qiu, Y.; Jiang, B.; Chen, Z.; Zhao, C.; Zhou, H.; Yang, L.; Fan, L.; Zhang, Y.; Zhang, N. Isolated Fe-Co heteronuclear diatomic sites as efficient bifunctional catalysts for high-performance lithium-sulfur batteries. *Nat. Commun.* **2023**, *14*, 291. [CrossRef]
40. Li, S.; Lin, J.; Chang, B.; Yang, D.; Wu, D.-Y.; Wang, J.; Zhou, W.; Liu, H.; Sun, S.; Zhang, L. Implanting single-atom N$_2$-Fe-B$_2$ catalytic sites in carbon hosts to stabilize high-loading and lean-electrolyte lithium-sulfur batteries. *Energy Storage Mater.* **2023**, *55*, 94–104. [CrossRef]
41. Ma, L.; Zhuang, H.L.; Wei, S.; Hendrickson, K.E.; Kim, M.S.; Cohn, G.; Hennig, R.G.; Archer, L.A. Enhanced Li–S batteries using amine-functionalized carbon nanotubes in the cathode. *ACS Nano* **2016**, *10*, 1050–1059. [CrossRef]

42. Wasalathilake, K.C.; Roknuzzaman, M.; Ostrikov, K.; Ayoko, G.A.; Yan, C. Interaction between functionalized graphene and sulfur compounds in a lithium–sulfur battery–A density functional theory investigation. *RSC Adv.* **2018**, *8*, 2271–2279. [CrossRef] [PubMed]

43. Cai, C.; Tao, Z.; Zhu, Y.; Tan, Y.; Wang, A.; Zhou, H.; Yang, Y.-Y. A nano interlayer spacing and rich defect 1T-MoS$_2$ as cathode for superior performance aqueous zinc-ion batteries. *Nanoscale Adv.* **2021**, *3*, 3780–3787. [CrossRef] [PubMed]

44. Li, H.; Han, X.; Jiang, S.; Zhang, L.; Ma, W.; Ma, R.; Zhou, Z. Controllable fabrication and structure evolution of hierarchical 1T-MoS$_2$ nanospheres for efficient hydrogen evolution. *Green Energy Environ.* **2022**, *7*, 314–323. [CrossRef]

45. Kızılaslan, A.; Çetinkaya, T.; Akbulut, H. 2H-MoS$_2$ as an artificial solid electrolyte interface in all-solid-state lithium–sulfur batteries. *Adv. Mat. Interfaces* **2020**, *7*, 2001020. [CrossRef]

46. Versaci, D.; Canale, I.; Goswami, S.; Amici, J.; Francia, C.; Fortunato, E.; Martins, R.; Pereira, L.; Bodoardo, S. Molybdenum disulfide/polyaniline interlayer for lithium polysulphide trapping in lithium-sulphur batteries. *J. Power Sources* **2022**, *521*, 230945. [CrossRef]

47. Liu, Y.; Cui, C.; Liu, Y.; Liu, W.; Wei, J. Application of MoS$_2$ in the cathode of lithium sulfur batteries. *RSC Adv.* **2020**, *10*, 7384–7395. [CrossRef] [PubMed]

48. Dong, S.; Sun, X.; Wang, Z. Trapping polysulfide on two-dimensional molybdenum disulfide for Li–S batteries through phase selection with optimized binding. *Beilstein J. Nanotechnol.* **2019**, *10*, 774–780. [CrossRef] [PubMed]

49. Teng, Y.; Zhao, H.; Zhang, Z.; Li, Z.; Xia, Q.; Zhang, Y.; Zhao, L.; Du, X.; Du, Z.; Lv, P.; et al. MoS$_2$ Nanosheets vertically grown on graphene sheets for lithium-ion battery anodes. *ACS Nano* **2016**, *10*, 8526–8535. [CrossRef]

50. You, Y.; Ye, Y.; Wei, M.; Sun, W.; Tang, Q.; Zhang, J.; Chen, X.; Li, H.; Xu, J. Three-dimensional MoS$_2$/rGO foams as efficient sulfur hosts for high-performance lithium-sulfur batteries. *Chem. Eng. J.* **2019**, *355*, 671–678. [CrossRef]

51. Du, Z.; Guo, Y.; Wang, H.; Gu, J.; Zhang, Y.; Cheng, Z.; Li, B.; Li, S.; Yang, S. High-Throughput Production of 1T MoS$_2$ Monolayers Based on Controllable Conversion of Mo-Based MXenes. *ACS Nano* **2021**, *15*, 19275–19283. [CrossRef] [PubMed]

52. Xu, Z.-L.; Onofrio, N.; Wang, J. Boosting the anchoring and catalytic capability of MoS$_2$ for high-loading lithium sulfur batteries. *J. Mater. Chem. A* **2020**, *8*, 17646–17656. [CrossRef]

53. Chen, D.; Zhan, W.; Fu, X.; Zhu, M.; Lan, J.; Sui, G.; Yang, X. High-conductivity 1T-MoS$_2$ catalysts anchored on a carbon fiber cloth for high-performance lithium–sulfur batteries. *Mater. Chem. Front.* **2021**, *5*, 6941–6950. [CrossRef]

54. Moon, S.-H.; Kim, M.-C.; Choi, J.-H.; Kim, Y.-S.; Kim, H.; Park, K.-W. 1T-MoS$_2$/carbon nanofiber composite as an interlayer fabricated by an in situ electrochemical fabrication method for lithium-sulfur batteries. *J. Alloys Compd.* **2021**, *857*, 158236. [CrossRef]

55. He, J.; Hartmann, G.; Lee, M.; Hwang, G.S.; Chen, Y.; Manthiram, A. Freestanding 1T MoS$_2$/graphene heterostructures as a highly efficient electrocatalyst for lithium polysulfides in Li–S batteries. *Energy Environ. Sci.* **2019**, *12*, 344–350. [CrossRef]

56. Yu, B.; Chen, Y.; Wang, Z.; Chen, D.; Wang, X.; Zhang, W.; He, J.; He, W. 1T-MoS$_2$ nanotubes wrapped with N-doped graphene as highly-efficient absorbent and electrocatalyst for Li–S batteries. *J. Power Sources* **2020**, *447*, 227364. [CrossRef]

57. Wang, H.; Tran, D.; Qian, J.; Ding, F.; Losic, D. MoS$_2$/Graphene composites as promising materials for energy storage and conversion applications. *Adv. Mater. Interfaces* **2019**, *6*, 1900915. [CrossRef]

58. Wen, G.; Zhang, X.; Sui, Y.; Rao, K.; Liu, J.; Zhong, S.; Wu, L. PPy-encapsulated hydrangea-type 1T MoS$_2$ microspheres as catalytic sulfur hosts for long-life and high-rate lithium-sulfur batteries. *Chem. Eng. J.* **2022**, *430 Pt 3*, 133041. [CrossRef]

59. Wang, J.; Wang, L.; Li, Z.; Bi, J.; Shi, Q.; Song, H. Recent advances of metal groups and their heterostructures as catalytic materials for lithium-sulfur battery cathodes. *J. Electron. Mater.* **2023**, *52*, 3526–3548. [CrossRef]

60. Guo, X.; Song, E.; Zhao, W.; Xu, S.; Zhao, W.; Lei, Y.; Fang, Y.; Liu, J.; Huang, F. Charge self-regulation in 1T'''-MoS$_2$ structure with rich S vacancies for enhanced hydrogen evolution activity. *Nat. Commun.* **2022**, *13*, 5954. [CrossRef]

61. Zhao, Y.; Tang, M.T.; Wu, S.; Geng, J.; Han, Z.; Chan, K.; Gao, P.; Li, H. Rational design of stable sulfur vacancies in molybdenum disulfide for hydrogen evolution. *J. Catal.* **2020**, *382*, 320–328. [CrossRef]

62. Liu, B.; Ma, C.; Liu, D.; Yan, S. Sulfur-vacancy defective MoS$_2$ as a promising electrocatalyst for nitrogen reduction reaction under mild conditions. *ChemElectroChem* **2021**, *8*, 3030–3039. [CrossRef]

63. Li, M.; Sami, I.; Yang, J.; Li, J.; Kumar, R.V.; Chhowalla, M. Lithiated metallic molybdenum disulfide nanosheets for high-performance lithium–sulfur batteries. *Nat. Energy* **2023**, *8*, 84–93. [CrossRef]

64. George, C.; Morris, A.J.; Modarres, M.H.; De Volder, M. Structural evolution of electrochemically lithiated MoS$_2$ nanosheets and the role of carbon additive in li-ion batteries. *Chem. Mater.* **2016**, *28*, 7304–7310. [CrossRef]

65. Lane, C.; Cao, D.; Li, H.; Jiao, Y.; Barbiellini, B.; Bansil, A.; Zhu, H. Understanding phase stability of metallic 1T-MoS$_2$ anodes for sodium-ion batteries. *Condens. Matter* **2019**, *4*, 53. [CrossRef]

66. Lee, W.S.V.; Xiong, T.; Wang, X.; Junmin Xue, J. Unraveling MoS$_2$ and transition metal dichalcogenides as functional zinc-ion battery cathode: A perspective. *Small Methods* **2021**, *5*, 2000815. [CrossRef] [PubMed]

67. Larson, D.T.; Fampiou, I.; Kim, G.; Kaxiras, E. Lithium intercalation in graphene–MoS$_2$ heterostructures. *J. Phys. Chem. C* **2018**, *122*, 24535–24541. [CrossRef]

68. Yang, F.; Feng, X.; Glans, P.-A.; Guo, J. MoS$_2$ for beyond lithium-ion batteries. *APL Mater.* **2021**, *9*, 050903. [CrossRef]

69. Wang, H.; Lu, Z.; Xu, S.; Kong, D.; Cha, J.J.; Zheng, G.; Hsu, P.-C.; Yan, K.; Bradshaw, D.; Prinz, F.B. Electrochemical tuning of vertically aligned MoS$_2$ nanofilms and its application in improving hydrogen evolution reaction. *Proc. Natl. Acad. Sci. USA* **2013**, *110*, 19701–19706. [CrossRef]

70. Zhang, J.; Yang, A.; Wu, X.; van de Groep, J.; Tang, P.; Li, S.; Liu, B.; Shi, F.; Wan, J.; Li, Q.; et al. Reversible and selective ion intercalation through the top surface of few-layer MoS$_2$. *Nat. Commun.* **2018**, *9*, 5289. [CrossRef]

71. El Garah, M.; Bertolazzi, S.; Ippolito, S.; Eredia, M.; Janica, I.; Melinte, G.; Ersen, O.; Marletta, G.; Ciesielski, A.; Samorì, P. MoS$_2$ nanosheets via electrochemical lithium-ion intercalation under ambient conditions. *FlatChem* **2018**, *9*, 33–39. [CrossRef]

72. Wang, X.; Guan, Z.; Li, Y.; Wang, Z.; Chen, L. Guest–host interactions and their impacts on structure and performance of nano-MoS$_2$. *Nanoscale* **2015**, *7*, 637–641. [CrossRef]

73. Zhao, X.; Hu, C.; Cao, M. Three-Dimensional MoS$_2$ hierarchical nanoarchitectures anchored into a carbon layer as graphene analogues with improved lithium ion storage performance. *Chem. Asian J.* **2013**, *8*, 2701–2707. [CrossRef]

74. Palencia-Ruiz, S.; Uzio, D.; Legens, C.; Laurenti, D.; Afanasiev, P. Stability and catalytic properties of 1T-MoS$_2$ obtained via solvothermal synthesis. *Appl. Catal. A Gen.* **2021**, *626*, 118355. [CrossRef]

75. Ali, L.; Bang, S.; Lee, Y.J.; Byeon, C.C. Ion-intercalation assisted solvothermal synthesis and optical characterization of MoS$_2$ quantum dots. *J. Korean Phys. Soc.* **2019**, *74*, 191–195. [CrossRef]

76. Fan, X.; Xu, P.; Zhou, D.; Sun, Y.; Li, Y.C.; Nguyen, M.A.T.; Terrones, M.; Mallouk, T.E. Fast and efficient preparation of exfoliated 2H MoS$_2$ nanosheets by sonication-assisted lithium intercalation and infrared laser-induced 1T to 2H phase reversion. *Nano Lett.* **2015**, *15*, 5956–5960. [CrossRef] [PubMed]

77. Haddadi, S.A.; Amini, M.; Ghaderi, S.; Ramazani, A.S.A. Synthesis and cation-exchange behavior of expanded MoS$_2$ nanosheets for anticorrosion applications. *Mater. Proc.* **2018**, *5*, 15573–15579.

78. Wang, L.; Xu, Z.; Wang, W.; Bai, X. Atomic mechanism of dynamic electrochemical lithiation processes of MoS$_2$ nanosheets. *J. Am. Chem. Soc.* **2014**, *136*, 6693–6697. [CrossRef] [PubMed]

79. Enyashin, A.N.; Seifert, G. Density-functional study of Li$_x$MoS$_2$ intercalates ($0 \leq x \leq 1$). *Comput. Theor. Chem.* **2012**, *999*, 13–20. [CrossRef]

80. Wu, L.; Dzade, N.Y.; Yu, M.; Mezari, B.; van Hoof, A.J.F.; Friedrich, H.; de Leeuw, N.H.; Hensen, E.J.M.; Hofmann, J.P. Unraveling the role of lithium in enhancing the hydrogen evolution activity of MoS$_2$: Intercalation versus adsorption. *ACS Energy Lett.* **2019**, *4*, 1733–1740. [CrossRef]

81. Zheng, Y.; Huang, Y.; Shu, H.; Zhou, X.; Ding, J.; Chen, X.; Lu, W. The effect of lithium adsorption on the formation of 1T-MoS$_2$ phase based on first-principles calculation. *Phys. Lett. A* **2016**, *380*, 1767–1771. [CrossRef]

82. Chen, S.; Wang, L.; Shao, R.; Zou, J.; Cai, R.; Lin, J.; Zhu, C.; Zhang, J.; Xu, F.; Cao, J.; et al. Atomic structure and migration dynamics of MoS$_2$/Li$_x$MoS$_2$ interface. *Nano Energy* **2018**, *48*, 560–568. [CrossRef]

83. Li, H.; Li, Y.; Zhang, L. Designing principles of advanced sulfur cathodes toward practical lithium-sulfur batteries. *SusMat* **2022**, *2*, 34–64. [CrossRef]

84. Pang, Q.; Liang, X.; Kwok, C.Y.; Nazar, L.F. Advances in lithium–sulfur batteries based on multifunctional cathodes and electrolytes. *Nat. Energy* **2016**, *1*, 16132. [CrossRef]

85. Mori, R. Cathode materials for lithium-sulfur battery: A review. *J. Solid State Electrochem.* **2023**, *27*, 813–839. [CrossRef]

86. Shuai, J.; Yoo, H.D.; Liang, Y.; Li, Y.; Yao, Y.; Grabow, L.C. Density functional theory study of Li, Na, and Mg intercalation and diffusion in MoS$_2$ with controlled interlayer spacing. *Mater. Res. Express* **2016**, *3*, 64001. [CrossRef]

87. Attanayake, N.H.; Thenuwara, A.C.; Patra, A.; Aulin, Y.V.; Tran, T.; Chakraborty, H.; Borguet, E.; Klein, M.L.; Perdew, J.P.; Strongin, D.R. Effect of intercalated metals on the electrocatalytic activity of 1T-MoS$_2$ for the hydrogen evolution reaction. *ACS Energy Lett.* **2018**, *3*, 7–13. [CrossRef]

88. Sun, D.; Huang, D.; Wang, H.; Xu, G.-L.; Zhang, X.; Zhang, R.; Tang, Y.; EI-Hady, D.A.; Alshitari, W.; AL-Bogami, A.S.; et al. 1T MoS$_2$ nanosheets with extraordinary sodium storage properties via thermal-driven ion intercalation assisted exfoliation of bulky MoS$_2$. *Nano Energy* **2019**, *61*, 361–369. [CrossRef]

89. Xu, J.; Zhang, J.; Zhang, W.; Lee, C.-S. Interlayer nanoarchitectonics of two-dimensional transition-metal dichalcogenides nanosheets for energy storage and conversion applications. *Adv. Energy Mater.* **2017**, *7*, 1700571. [CrossRef]

90. Grabe, S.; Dent, M.; Babar, S.; Zhang, T.; Tennison, S.; Watts, J.F.; Lekakou, C. Investigation and determination of electrochemical reaction kinetics in lithium-sulfur batteries with electrolyte LiTFSI in DOL/DME. *J. Electrochem. Soc.* **2023**, *170*, 020527. [CrossRef]

91. Liu, Y.; Elias, Y.; Meng, J.; Aurbach, D.; Zou, R.; Xia, D.; Pang, Q. Electrolyte solutions design for lithium-sulfur batteries. *Joule* **2021**, *5*, 2323–2364. [CrossRef]

92. Lu, Y.-C.; He, Q.; Gasteiger, H.A. Probing the lithium−sulfur redox reactions: A rotating-ring disk electrode study. *J. Phys. Chem. C* **2014**, *118*, 5733. [CrossRef]

93. Ponnada, S.; Kiai, M.S.; Gorle, D.B.; Nowduri, A. History and recent developments in divergent electrolytes towards high-efficiency lithium–sulfur batteries–A review. *Mater. Adv.* **2021**, *2*, 4115–4139. [CrossRef]

94. Acerce, M.; Akdoan, E.K.; Chhowalla, M. Metallic molybdenum disulfide nanosheet-based electrochemical actuators. *Nature* **2017**, *549*, 370–373. [CrossRef] [PubMed]

95. Acerce, M.; Voiry, D.; Chhowalla, M. Metallic 1T phase MoS$_2$ nanosheets as supercapacitor electrode materials. *Nat. Nanotechnol.* **2015**, *10*, 313–318. [CrossRef] [PubMed]

96. Zhao, C.; Xu, G.-L.; Yu, Z.; Zhang, L.; Hwang, I.; Mo, Y.-X.; Ren, Y.; Cheng, L.; Sun, C.-J.; Ren, Y.; et al. A high-energy and long-cycling lithium–sulfur pouch cell via a macroporous catalytic cathode with double-end binding sites. *Nat. Nanotechnol.* **2021**, *16*, 166–173. [CrossRef] [PubMed]

97. Clark, S.J.; Segall, M.D.; Pickard, C.J.; Hasnip, P.J.; Probert, M.I.J.; Refson, K.; Payne, M.C. First principles methods using CASTEP. *Z. Kristallogr. Cryst. Mater.* **2005**, *220*, 567–570. [CrossRef]

98. Roch, J.G.; Froehlicher, G.; Leisgang, N.; Makk, P.; Watanabe, K.; Taniguchi, T.; Warburton, R.J. Spin-polarized electrons in monolayer MoS$_2$. *Nat. Nanotechnol.* **2019**, *14*, 432–436. [CrossRef] [PubMed]

99. Bouarissa, A.; Gueddim, A.; Bouarissa, N.; Maghraoui-Meherzi, H. Optical spectra of monolayer MoS$_2$ from spin-polarized all electrons density-functional calculations. *Optik* **2020**, *222*, 165477. [CrossRef]

100. Blöchl, P.E. Projector augmented-wave method. *Phys. Rev. B* **1994**, *50*, 17953. [CrossRef]

101. Grimme, S. Semiempirical GGA-type density functional constructed with a long-range dispersion correction. *J. Comput. Chem.* **2006**, *27*, 1787–1799. [CrossRef]

102. Xu, B.; Wang, L.; Chen, H.J.; Zhao, J.; Liu, G.; Wu, M.S. Adsorption and diffusion of lithium on 1T-MoS$_2$ monolayer. *Comput. Mater. Sci.* **2014**, *93*, 86–90. [CrossRef]

103. Zeradjanin, A.R.; Narangoda, P.; Masa, J.; Schlögl, R. What controls activity trends of electrocatalytic hydrogen evolution reaction?—Activation energy versus frequency factor. *ACS Catal.* **2022**, *12*, 11597–11605. [CrossRef]

104. Roduner, E. Understanding catalysis. *Chem. Soc. Rev.* **2014**, *43*, 8226–8239. [CrossRef] [PubMed]

105. Wang, Y.; Qiu, W.; Song, E.; Gu, F.; Zheng, Z.; Zhao, X.; Zhao, Y.; Liu, J.; Zhang, W. Adsorption-energy-based activity descriptors for electrocatalysts in energy storage applications. *Natl. Sci. Rev.* **2018**, *5*, 327–341. [CrossRef]

106. Darby, M.T.; Reocreux, R.; Sykes, E.C.H.; Michaelides, A.; Stamatakis, M. Elucidating the stability and reactivity of surface intermediates on single atom alloy catalysts. *ACS Catal.* **2018**, *8*, 5038–5050. [CrossRef]

107. Yu, H.; Wang, Z.; Ni, J.; Li, L. Freestanding nanosheets of 1T-2H hybrid MoS$_2$ as electrodes for efficient sodium storage. *J. Mater. Sci. Technol.* **2021**, *67*, 237–242. [CrossRef]

108. Yu, H.; Jiang, G.; Ni, J.; Li, L. Architecting core-shell nanosheets of MoS$_2$-polypyrrole on carbon cloth as a robust sodium anode. *Sustain. Mater. Technol.* **2021**, *28*, e00255. [CrossRef]